Pure Appl. Chem., Vol. 78, No. 12, pp. 2267–2276, 2006.
doi:10.1351/pac200678122267

Overall water splitting using (oxy)nitride photocatalysts*

Kazuhiko Maeda[1], Kentaro Teramura[1], Nobuo Saito[2], Yasunobu Inoue[2], Hisayoshi Kobayashi[3], and Kazunari Domen[1,4,‡]

[1]Department of Chemical System Engineering, The University of Tokyo, 7-3-1 Hongo, Bunkyo-ku, Tokyo 113-8656, Japan; [2]Department of Chemistry, Nagaoka University of Technology, Nagaoka 940-2188, Japan; [3]Department of Chemistry and Materials Technology, Faculty of Engineering and Design, Kyoto Institute of Technology, Goshokaido-cho, Matsugasaki, Sakyo-ku, Kyoto 606-8585, Japan; [4]Solution Oriented Research for Science and Technology (SORST) programs of the Japan Science and Technology Agency (JST), 4-1-8 Honcho, Kawaguchi-shi, Saitama 332-0012, Japan

Abstract: Oxynitride photocatalysts with d^{10} electronic configuration are presented as effective non-oxide catalysts for overall water splitting. Germanium nitride (β-Ge_3N_4) having a band gap of 3.8–3.9 eV modified with RuO_2 nanoparticles as a cocatalyst is shown to achieve stoichiometric decomposition of H_2O into H_2 and O_2 under UV irradiation ($\lambda > 200$ nm). A novel solid solution of GaN and ZnO, $(Ga_{1-x}Zn_x)(N_{1-x}O_x)$, with a band gap of 2.4–2.8 eV (depending on composition) achieves overall water splitting under visible light ($\lambda > 400$ nm) when loaded with an appropriate cocatalyst. The narrower band gap of the solid solution is attributed to the bonding between Zn and N atoms at the top of the valence band. The photocatalytic activity of $(Ga_{1-x}Zn_x)(N_{1-x}O_x)$ for overall water splitting is strongly dependent on both the cocatalyst and the crystallinity and composition of the material. The quantum efficiency of $(Ga_{1-x}Zn_x)(N_{1-x}O_x)$ with Rh and Cr mixed-oxide nanoparticles is 2–3 % at 420–440 nm, which is the highest reported efficiency for overall water splitting in the visible-light region.

Keywords: water splitting; oxynitride; photocatalyst; hydrogen; visible light.

INTRODUCTION

In recent years, photocatalytic materials that function under visible light have been studied extensively in an attempt to improve solar energy conversion and reduce the environmental impact of energy production. Research on direct water splitting with photon energy was pioneered by Honda and Fujishima, who demonstrated a photoelectrochemical (PEC) cell consisting of a Pt cathode and TiO_2 (rutile) as a photoanode [1]. Many PEC cells have since been proposed, and the efficiency of solar energy conversion achieved by such devices has improved. However, due to the lack of photoelectrode materials with suitable band gap structures and adequate stability, PEC systems have remained rather complex, requiring integration of multiple layers or tandem systems [2,3]. Overall water splitting using particulate

*Paper based on a presentation at the XXI[st] IUPAC Symposium on Photochemistry, 2–7 April 2006, Kyoto, Japan. Other presentations are published in this issue, pp. 2193–2359.

‡Corresponding author: Tel.: +81-3-5841-1148; Fax: +81-3-5841-8838; E-mail: domen@chemsys.t.u-tokyo.ac.jp; Present address: Department of Chemical System Engineering, The University of Tokyo, 7-3-1 Hongo, Bunkyo-ku, Tokyo 113-8656, Japan.

photocatalysts, somewhat similar to the photosynthetic reaction, have also been examined since 1980 [4–6]. Over the last two decades, a number of metal-oxide photocatalysts, including TiO_2 [4], $SrTiO_3$ [5,6], $K_4Nb_6O_{17}$ [7,8], $NaTaO_3$ [9], $CaIn_2O_4$ [10], and Zn_2GeO_4 [11] have been demonstrated to be effective for photocatalytic overall water splitting, and some have achieved quantum efficiencies of greater than 50 % [12]. Most of the metal-oxide photocatalysts developed to date, however, only function in the UV region due to their large band gap energies (>3 eV) [13]. Although some non-oxide materials (e.g., CdS and CdSe) have been examined as visible-light-driven photocatalysts, overall water splitting using these materials has not hitherto been achieved due to the inherent instability of these materials for water oxidation via the photogeneration of holes [14,15]. From the viewpoint of large-scale application, a simple photocatalytic overall water-splitting reaction system is considered to be advantageous [16] over more complex multilayer or tandem structure devices [2,3], although a method for the separation of simultaneously produced H_2 and O_2 is required. The development of an efficient photocatalyst for visible-light-driven overall water splitting therefore remains a challenge.

The two major obstacles to the development of powder photocatalysts are the discovery of new stable photocatalytic materials and the construction of a suitable visible-light-driven photocatalyst system. The application of metal oxides for photocatalysis in the visible-light region is complicated by the deep valence band positions (O2p orbitals) of these materials, resulting in a band gap that is too large to absorb visible light. Since the N2p orbital has a higher potential energy than the O2p orbital, it would be interesting to use a metal nitride or metal oxynitride as a photocatalyst. The authors recently reported oxynitrides, such as TaON [17], Ta_3N_5 [18], and $LaTiO_2N$ [19] as potential candidates for overall water splitting under visible light. However, overall water splitting over these oxynitrides has not been hitherto achieved due at least in part to the relatively high densities of defects in the bulk and at the surfaces of these materials. These (oxy)nitrides are composed of transition-metal cations of Ti^{4+}, Nb^{5+}, or Ta^{5+}, which have an empty d orbital. We define a photocatalyst that contains such transition-metal cations as a "d^0 electronic configuration" photocatalyst. On the other hand, from the viewpoint of electronic band structure, semiconductors that contain typical metal cations, such as Ga^{3+} and Ge^{4+}, with a filled d orbital (defined as "d^{10} electronic configuration" photocatalysts) have an advantage as a photocatalyst, compared to materials with d^0 electronic configuration [10,11]. The top of the valence band for transition-metal oxides with d^0 electronic configuration consists of O2p orbitals, whereas the bottom of the conduction band is composed of empty d orbitals of the transition metals. In typical metal oxides with d^{10} electronic configuration, however, the bottom of the conduction band consists of hybridized s,p orbitals of the metals, although the valence band is formed essentially by O2p orbitals. The hybridized s,p orbitals possess large dispersion, increasing the mobility of photogenerated electrons in the conduction band and promoting photocatalytic activity [10,11]. Oxynitrides with d^{10} electronic configuration are, therefore, of interest as potentially efficient photocatalysts for overall water splitting. In the present paper, new oxynitride-type photocatalysts with d^{10} electronic configuration are presented.

β-Ge_3N_4 [20]

A typical metal nitride with d^{10} electronic configuration, β-Ge_3N_4, was synthesized from GeO_2 powder by nitridation under a flow of NH_3 at 1153 K for 10 h. Transmission electron microscopy (TEM) images and an electron diffraction pattern of the as-prepared β-Ge_3N_4 are shown in Fig. 1. The figure clearly reveals that the sample consisted of primary well-crystallized submicrometer-order particles with a hexagonal crystal system, as indicated by the lattice fringe and electron diffraction patterns.

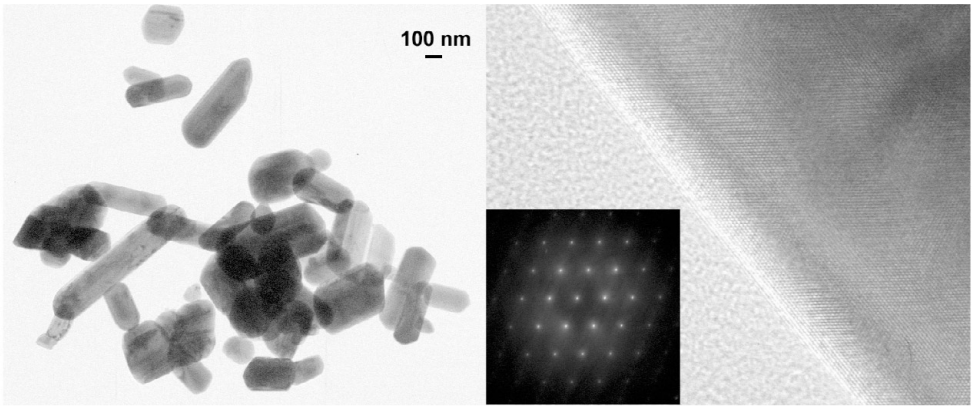

Fig. 1 TEM images and electron diffraction patterns of β-Ge_3N_4.

The photocatalytic activity of the as-prepared β-Ge_3N_4 for overall water splitting is negligible. However, when modified with RuO_2 nanoparticles, the material became photocatalytically active. The photocatalytic activity increased remarkably as the amount of loaded RuO_2 was increased, reaching maximum activity when loaded with 1 wt % RuO_2. Figure 2 shows scanning electron microscopy (SEM) and TEM images of the 1 wt % RuO_2-loaded β-Ge_3N_4. The images reveal that RuO_2 nanoparticles of 20–50 nm in size are distributed uniformly on the β-Ge_3N_4 surface, and the lattice fringes in the TEM image indicate that the loaded RuO_2 nanoparticles are crystalline. The RuO_2 nanoparticles dispersed on the β-Ge_3N_4 surface work as a water reduction promoter, as discussed in previous work [11]. The photocatalytic performance of the RuO_2-loaded β-Ge_3N_4 was found to be strongly dependent on the pH of the reactant solution. The activity increased with decreasing pH from 7 to a maximum at pH 0. N_2 evolution, indicative of the partial decomposition of the nitride photocatalyst, was observed in the initial stage of reaction at pH 7, but was almost entirely suppressed at pH 0. This characteristic pH dependence of the RuO_2-loaded β-Ge_3N_4 photocatalyst deviates significantly from the general character of photocatalysts based on transition-metal oxides [9], and is thus of particular interest. A typical time course of overall water splitting using the 1 wt % RuO_2-loaded β-Ge_3N_4 catalyst at pH 0 is presented in Fig. 3. Both H_2 and O_2 evolved stoichiometrically from the beginning of the reaction. The total amount of H_2 and O_2 evolved over 5 h was 6.7 mmol, substantially greater than the amount of catalyst (0.5 g; 1.8 mmol of β-Ge_3N_4). No noticeable change in the X-ray diffraction (XRD) patterns was observed as a result of the reaction. These results clearly demonstrate that RuO_2-loaded β-Ge_3N_4 is a suitable photocatalyst for overall water splitting. The quantum efficiency of water splitting on RuO_2-loaded β-Ge_3N_4 is roughly estimated to be ca. 9 % at an excitation wavelength of 300 nm.

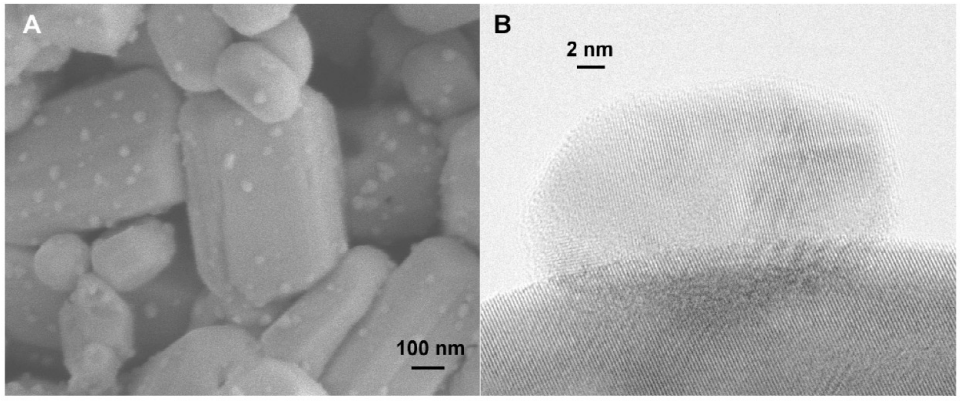

Fig. 2 (A) SEM and (B) TEM images of 1 wt % RuO_2-loaded β-Ge_3N_4.

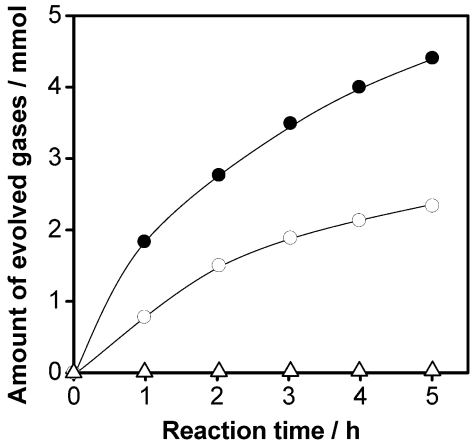

Fig. 3 Time course of overall water splitting using 1 wt % RuO_2-loaded β-Ge_3N_4 at pH 0 under UV irradiation ($\lambda >$ 200 nm). Solid circles denote H_2 production, open circles denote O_2, and triangles denote N_2.

Figure 4 shows the UV–vis diffuse reflectance spectrum for β-Ge_3N_4. Two absorption bands are apparent in the spectrum; a strong absorption in the UV region shorter than 340 nm, and a broad absorption extending into the visible region. The band gap of β-Ge_3N_4 is estimated to be 3.8–3.9 eV based on the onset of the diffuse reflectance spectrum. The absorption at longer wavelengths of up to 700–800 nm is considered to be due to impurities and defect sites. Such impurities or defects are attributed to reduced Ge species (Ge^0, Ge^{2+}) produced by H_2 derived from the disassociation of NH_3 at high temperature. No appreciable evolution of H_2 or O_2 was observed under irradiation at longer wavelengths.

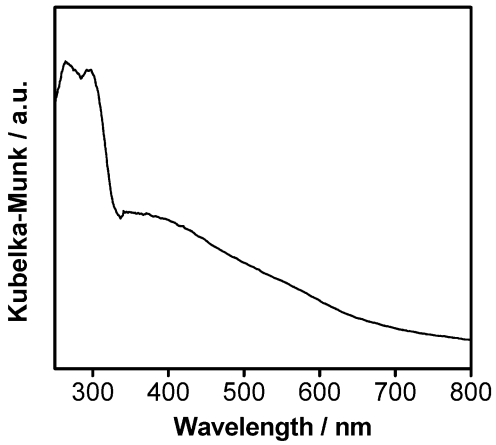

Fig. 4 UV–vis diffuse reflectance spectrum for β-Ge_3N_4.

The electronic structure of β-Ge_3N_4 was investigated through plane-wave density functional theory (DFT) calculations. Figure 5 shows the energy band dispersion and density of states (DOS) for this composition. Density contour maps for the top of the valence band (highest occupied molecular orbital, HOMO) and the bottom of the conduction band (lowest unoccupied molecular orbital, LUMO) are also shown. The DOS indicates that the top of the valence band consists of N2p orbitals, and that the bottom of the conduction band is composed of hybridized Ge4s,4p orbitals with slight mixing of N2p orbitals. This result indicates that photoexcitation under irradiation occurs via transition from the N2p orbitals to the Ge4s,4p hybridized orbitals. Water oxidation to produce O_2 over conventional metal-oxide photocatalysts takes place as a result of contributions from photogenerated holes in the valence band consisting of O2p orbitals. It is noteworthy that the N2p orbitals in the valence band are also able to photogenerate holes and thereby contribute to photocatalytic water oxidation.

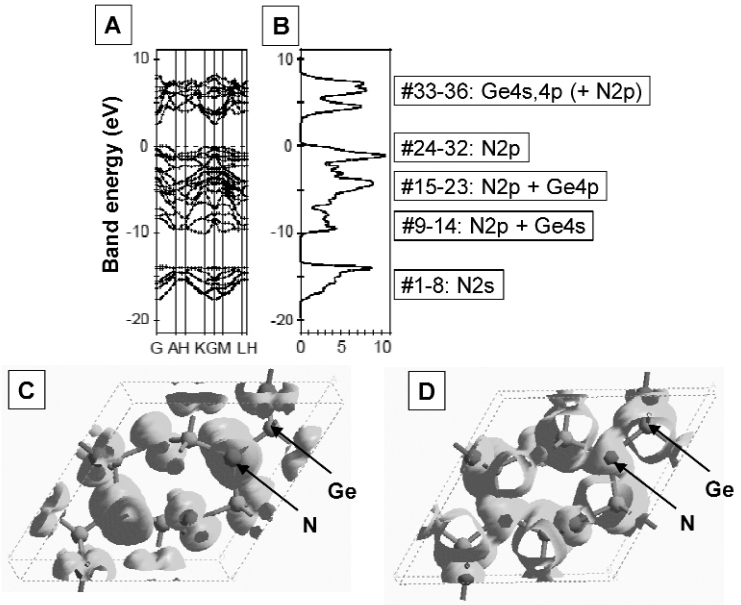

Fig. 5 DFT calculations for β-Ge_3N_4: (A) energy band dispersion, (B) DOS, and density contour maps for (C) the valence band maximum (HOMO) and (D) the conduction band minimum (LUMO) .

$(Ga_{1-x}Zn_x)(N_{1-x}O_x)$ SOLID SOLUTION [21–25]

Further research on d^{10}-type metal oxynitrides revealed that a solid solution of GaN and ZnO, denoted $(Ga_{1-x}Zn_x)(N_{1-x}O_x)$, functions as a photocatalyst for the decomposition of H_2O to H_2 and O_2 under visible-light irradiation. $(Ga_{1-x}Zn_x)(N_{1-x}O_x)$ is of interest not only as a novel photocatalyst but also as a new type of material.

Both GaN and ZnO are important III–V and II–VI semiconductors, and have been studied extensively for application in light-functional materials such as light-emitting diodes and laser diodes [26–28]. The $(Ga_{1-x}Zn_x)(N_{1-x}O_x)$ solid solution possesses a wurtzite crystal structure similar to GaN and ZnO, and is typically synthesized by nitriding a mixture of Ga_2O_3 and ZnO. Elemental analyses by inductive coupled plasma optical emission spectroscopy (ICP-OES) has revealed that the ratios of Ga to N (Ga/N) and Zn to O (Zn/O) in the $(Ga_{1-x}Zn_x)(N_{1-x}O_x)$ are close to unity and that the N and O concentrations increase with the Ga and Zn concentrations. Figure 6 shows the XRD patterns of samples with different compositions. All examples exhibit single-phase diffraction patterns indicative of the wurtzite structure similar to GaN and ZnO. The position of the d(100) diffraction peak was successively shifted to lower angles (2θ) with increasing Zn and O concentrations, indicating that the obtained samples were not physical mixtures of GaN and ZnO phases, but solid solutions of GaN and ZnO. This peak shift is reasonable, as the ionic radius of Zn^{2+} (0.74 Å) is larger than that of Ga^{3+} (0.61 Å) [29]. The same tendency was confirmed by Rietveld analysis. Furthermore, neutron diffraction analysis revealed that O substitutes for N in the crystal structure of $(Ga_{1-x}Zn_x)(N_{1-x}O_x)$.

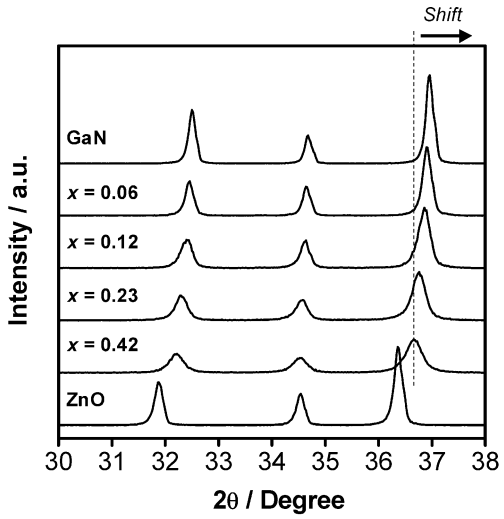

Fig. 6 Powder XRD patterns for $(Ga_{1-x}Zn_x)(N_{1-x}O_x)$ with various compositions.

Figure 7 shows the UV–vis diffuse reflectance spectra for several samples. Whereas neither GaN nor ZnO absorb visible light due to their large band gap energies (>3 eV), the $(Ga_{1-x}Zn_x)(N_{1-x}O_x)$ solid solutions exhibit steep absorption edges in the visible-light region. The absorption edge shifts to longer wavelengths with increasing Zn and O concentrations (x) in $(Ga_{1-x}Zn_x)(N_{1-x}O_x)$. The band gap energies of the solid solutions are roughly estimated to be 2.4–2.8 eV based on the onsets of the diffuse reflectance spectra.

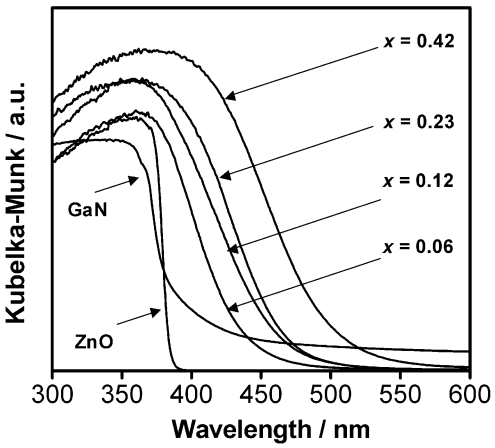

Fig. 7 UV–vis diffuse reflectance spectra for $(Ga_{1-x}Zn_x)(N_{1-x}O_x)$ with various compositions.

The energy band dispersion and DOS for $(Ga_{1-x}Zn_x)(N_{1-x}O_x)$ determined by DFT calculations are shown in Fig. 8. The results indicate that the bottom of the conduction band for $(Ga_{1-x}Zn_x)(N_{1-x}O_x)$ is mainly composed of hybridized Ga4s,4p orbitals, while the top of the valence band consists of N2p orbitals with lesser contributions of Zn3d and O2p orbitals. The DFT calculations also indicated that the bottom of the conduction band for GaN is composed of 4s and 4p orbitals of Ga, and that the top of the valence band consists of N2p orbitals. The presence of Zn3d and N2p electrons in the upper valence band for $(Ga_{1-x}Zn_x)(N_{1-x}O_x)$ provides p–d repulsion for the valence-band maximum, resulting in a narrowing of the band gap [30]. Thus, the visible-light response of the solid solution originates from the contribution of Zn3d atomic orbitals to the valence-band formation, where the bonding between Zn and N atoms is formed as a result of the formation of the solid solution.

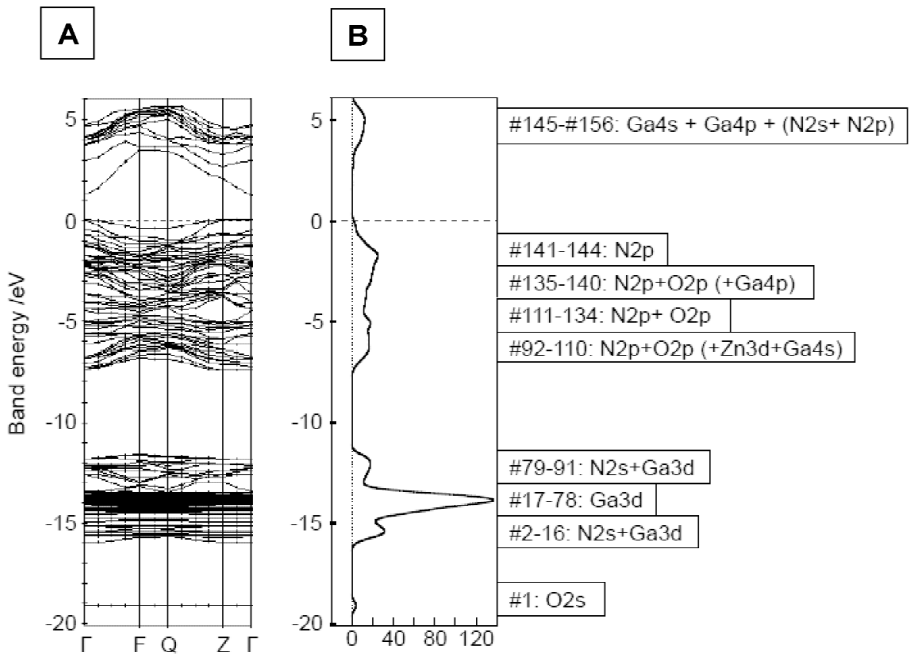

Fig. 8 DFT calculations for $(Ga_{1-x}Zn_x)(N_{1-x}O_x)$: (A) energy band dispersion, and (B) DOS.

The as-prepared $(Ga_{1-x}Zn_x)(N_{1-x}O_x)$ exhibits little photocatalytic activity for water decomposition even under UV irradiation. However, modification with RuO_2 nanoparticles results in clearly observable H_2 and O_2 evolution. This modification involves deposition of RuO_2 nanoparticles on the surface of the $(Ga_{1-x}Zn_x)(N_{1-x}O_x)$ as H_2 evolution sites. The photocatalytic activity increased remarkably with increasing RuO_2 content to a maximum at 5 wt % RuO_2, with the activity dropping gradually at higher RuO_2 concentrations. It was elucidated by SEM, X-ray photoelectron spectroscopy, and X-ray absorption spectroscopy that the enhancement of photocatalytic activity by RuO_2 loading is driven by the formation of crystalline RuO_2 nanoparticles, with the optimal particle size and coverage yielding the peak activity. The photocatalytic performance of the RuO_2-loaded $(Ga_{1-x}Zn_x)(N_{1-x}O_x)$ was also found to be strongly dependent on both the pH of the aqueous solution and the crystallinity and composition of $(Ga_{1-x}Zn_x)(N_{1-x}O_x)$. The activity increased with decreasing pH from pH 7, reaching maximum activity at pH 3. This tendency is similar to that observed above for RuO_2-loaded β-Ge_3N_4. The occurrence of peak activity in an acidic medium is consistent with the general characteristics of oxynitride materials, which are inherently unstable in basic media but stable in acidic media. Below pH 3, at which the activity began to decrease, the surface of the catalyst is no longer completely stable due to the corrosion of surface Zn species. It is known that O_2 evolution occurs over ZnO when employed as a photoanode for water oxidation in a PEC, accompanied by degradation of the ZnO [31]. It was confirmed by ^{18}O-isotopic H_2O cleavage that the O_2 evolution over the present catalyst is due to water oxidation, and the XRD patterns of the samples remained unchanged after the reaction. These results indicate that $(Ga_{1-x}Zn_x)(N_{1-x}O_x)$ functions as a stable visible-light-driven photocatalyst for overall water splitting.

The photocatalytic activity of $(Ga_{1-x}Zn_x)(N_{1-x}O_x)$ for overall water splitting was found to be dependent on the cocatalyst employed, as shown in Fig. 9. A mixed-oxide of Rh and Cr was the most effective for promoting overall water splitting. Interestingly, modification with either Rh or Cr oxide alone did not provide an appreciable increase in photocatalytic activity. Figure 10 shows the time course of overall water splitting using $(Ga_{1-x}Zn_x)(N_{1-x}O_x)$ modified with Rh and Cr mixed-oxide nanoparticles under visible-light irradiation ($\lambda > 400$ nm). Data for RuO_2-loaded $(Ga_{1-x}Zn_x)(N_{1-x}O_x)$ are provided for comparison. Although both catalysts evolved H_2 and O_2 steadily and stoichiometrically upon irradiation with visible light, the activity of $(Ga_{1-x}Zn_x)(N_{1-x}O_x)$ modified with Rh and Cr mixed-oxide was substantially higher than that of the RuO_2-loaded sample. Modification of $(Ga_{1-x}Zn_x)(N_{1-x}O_x)$ with Rh and Cr mixed-oxide nanoparticles increased the quantum efficiency for overall water splitting to 2–3 % at 420–440 nm, which is approximately 10 times greater than that achieved using the RuO_2-loaded catalyst. When the reaction is carried out in the presence of silver nitrate as a sacrificial electron acceptor, the quantum efficiency for water oxidation rises to 51 % at 420–440 nm. This indicates that more than 50 % of the photogenerated electrons and holes in the $(Ga_{1-x}Zn_x)(N_{1-x}O_x)$ bulk are available for the surface chemical reaction. It also appears possible to extend the absorption edge by changing the composition of the material. The performance of this catalyst can therefore be expected to improve through refinement of the preparation method and development of new effective modification methods.

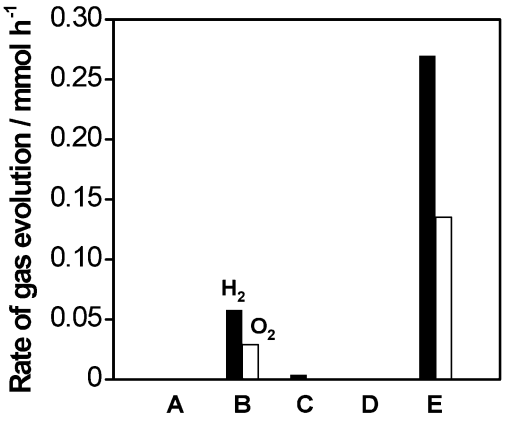

Fig. 9 Photocatalytic activities of $(Ga_{1-x}Zn_x)(N_{1-x}O_x)$ with various cocatalysts for overall water splitting under visible-light irradiation ($\lambda > 400$ nm): (A) no cocatalyst, (B) RuO_2, (C) Rh oxide, (D) Cr oxide, and (E) Rh–Cr mixed-oxide.

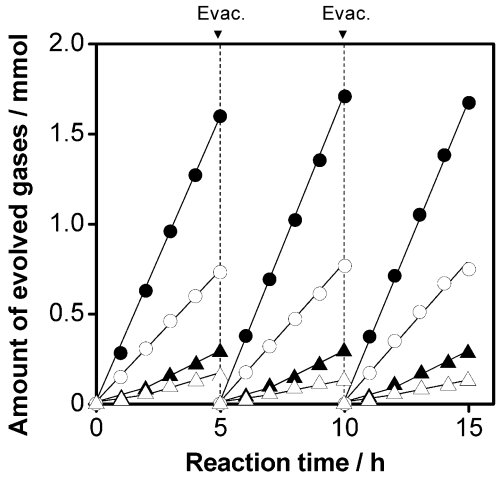

Fig. 10 Time courses of overall water splitting using $(Ga_{1-x}Zn_x)(N_{1-x}O_x)$ with various cocatalysts under visible-light irradiation ($\lambda > 400$ nm). Circles denote Rh–Cr mixed-oxide cocatalyst, triangles denote RuO_2, solid symbols denote H_2 production, open symbols denote O_2. Catalyst (0.3 g); an aqueous H_2SO_4 solution adjusted at pH 3.0 for RuO_2-loaded sample and at pH 4.5 for $Rh_{2-y}Cr_yO_3$-loaded sample (370 mL); light source, high-pressure mercury lamp (450 W); inner irradiation-type reaction vessel made of Pyrex with an aqueous $NaNO_2$ solution (2 M) filter.

CONCLUSION

β-Ge_3N_4 and $(Ga_{1-x}Zn_x)(N_{1-x}O_x)$ with d^{10} electronic configuration were presented as non-oxide photocatalysts for overall water splitting. $(Ga_{1-x}Zn_x)(N_{1-x}O_x)$ modified with RuO_2 or Rh and Cr mixed-oxide nanoparticles photocatalyze H_2O into H_2 and O_2 under visible-light irradiation. Although the quantum efficiency of the material is as yet too low for practical application, this is the first example of overall water splitting using a particulate photocatalyst with a band gap in the visible-light region. All of the successful photocatalysts developed for overall water splitting over the past 30 years have been comprised solely of metal oxides. The discovery of a non-oxide photocatalyst achieving the same function as the metal oxide is expected to stimulate research on non-oxide photocatalysts for solar energy conversion.

ACKNOWLEDGMENTS

This work was supported by the Solution Oriented Research for Science and Technology (SORST) program of the Japan Science and Technology (JST) Agency and the 21st Century Center of Excellence (COE) program of the Ministry of Education, Culture, Sports, Science and Technology of Japan.

REFERENCES

1. A. Fujishima, K. Honda. *Nature* **238**, 37 (1972).
2. Y. Sakai, S. Sugahara, M. Matsumura, Y. Nakato, H. Tsubomura. *Can. J. Chem.* **66**, 1853 (1988).
3. O. Khaselev, J. A. Turner. *Science* **280**, 425 (1998).
4. S. Sato, J. M. White. *Chem. Phys. Lett.* **72**, 83 (1980).
5. K. Domen, S. Naito, M. Soma, T. Onishi, K. Tamaru. *J. Chem. Soc., Chem. Commun.* 543 (1980).
6. J. M. Lehn, J. P. Sauvage, R. Ziessel. *Nouv. J. Chim.* **4**, 623 (1980).
7. K. Domen, A. Kudo, A. Shinozaki, A. Tanaka, K. Maruya, T. Onishi. *J. Chem. Soc., Chem. Commun.* 356 (1986).
8. A. Kudo, A. Tanaka, K. Domen, K. Maruya, K. Aika, T. Onishi. *J. Catal.* **111**, 67 (1988).
9. H. Kato, A. Kudo. *Catal. Lett.* **58**, 153 (1999).
10. J. Sato, N. Saito, H. Nishiyama, Y. Inoue. *J. Phys. Chem. B* **105**, 6061 (2001).
11. J. Sato, H. Kobayashi, K. Ikarashi, N. Saito, H. Nishiyama, Y. Inoue. *J. Phys. Chem. B* **108**, 4369 (2004).
12. H. Kato, K. Asakura, A. Kudo. *J. Am. Chem. Soc.* **125**, 3082 (2003).
13. D. E. Scaife. *Sol. Energy* **25**, 41 (1980).
14. R. Williams. *J. Chem. Phys.* **32**, 1505 (1960).
15. A. B. Ellis, S. W. Kaiser, J. M. Bolts, M. S. Wrighton. *J. Am. Chem. Soc.* **99**, 2839 (1977).
16. A. J. Bard, M. A. Fox. *Acc. Chem. Res.* **28**, 141 (1995).
17. G. Hitoki, T. Takata, J. N. Kondo, M. Hara, H. Kobayashi, K. Domen. *Chem. Commun.* 1698 (2002).
18. G. Hitoki, A. Ishikawa, T. Takata, J. N. Kondo, M. Hara, K. Domen. *Chem. Lett.* **31**, 736 (2002).
19. A. Kasahara, K. Nukumizu, G. Hitoki, T. Takata, J. N. Kondo, M. Hara, H. Kobayashi, K. Domen. *J. Phys. Chem. A* **106**, 6750 (2002).
20. J. Sato, N. Saito, Y. Yamada, K. Maeda, T. Takata, J. N. Kondo, M. Hara, H. Kobayashi, K. Domen. *J. Am. Chem. Soc.* **127**, 4150 (2005).
21. K. Maeda, T. Takata, M. Hara, N. Saito, Y. Inoue, H. Kobayashi, K. Domen. *J. Am. Chem. Soc.* **127**, 8286 (2005).
22. K. Maeda, K. Teramura, T. Takata, M. Hara, N. Saito, K. Toda, Y. Inoue, H. Kobayashi, K. Domen. *J. Phys. Chem. B* **109**, 20504 (2005).
23. K. Teramura, K. Maeda, T. Saito, T. Takata, N. Saito, Y. Inoue, K. Domen. *J. Phys. Chem. B* **109**, 21915 (2005).
24. M. Yashima, K. Maeda, K. Teramura, T. Takata, K. Domen. *Chem. Phys. Lett.* **416**, 225 (2005).
25. K. Maeda, K. Teramura, D. Lu, T. Takata, N. Saito, Y. Inoue, K. Domen. *Nature* **440**, 295 (2006).
26. S. Nakamura, T. Mukai, M. Senoh. *Appl. Phys. Lett.* **64**, 1687 (1994).
27. S. Nakamura. *Science* **281**, 956 (1998).
28. A. Tsukazaki, A. Ohtomo, T. Onuma, M. Ohtani, T. Makino, M. Sumiya, K. Ohtani, S. F. Chichibu, S. Fuke, Y. Segawa, H. Ohno, H. Koinuma, M. Kawasaki. *Nat. Mater.* **4**, 42 (2005).
29. R. D. Shannon. *Acta Crystallogr., Sect. A* **32**, 751 (1976).
30. S. K. Sampath, D. G. Kanhere, R. Pandey. *J. Phys.: Condens. Matter* **111**, 3635 (1999).
31. H. Gerischer. *J. Electrochem. Soc.* **113**, 1174 (1966).